A Novel Liquid Water Content Retrieval Method Based on Mass Absorption for Single-Wavelength Cloud Radar

Jinming Ge, Jiajing Du, Zheyu Liang, Zeen Zhu, Jing Su, Qinghao Li, Qingyu Mu, Jianping Huang, and Qiang Fu

***Abstract*— Low-level clouds (LLCs), mainly composed of liquid water droplets, cool the climate system by strongly reflecting solar radiation back to space and thus play an important role in the Earth energy budget. However, the LLC properties and their radiative effects are poorly represented in climate models, leading to the largest source of uncertainty in climate prediction. Liquid water content (LWC) is a key property of LLC determining cloud extinction characteristics and is a fundamental parameter in the radiative transfer model. To improve the understanding of LWC properties, algorithms have been proposed to retrieve LWC based on millimeter-wavelength radar. However, the traditional retrieval relies on preconstructed empirical relationship between reflectivity and LWC and has noticeable limitations. In particular, the retrieval uncertainty is strongly dependent on the assumed particle size distribution, the existence of drizzle particle, and on the accuracy of reflectivity measurement. In this study, we develop a new self-consistent algorithm to retrieve LWC by constraining radar reflectivity factor and attenuation in the whole liquid cloud layer. A relationship between the radar measured reflectivity, LWC, and intrinsic reflectivity is first constructed based on the radiative transfer theory under the Rayleigh scattering regime. A nonlinear least-square regression technique is then applied to derive the optimal parameters in the retrieval equations to obtain the LWC. Comparison with the microwave radiometer (MWR) derived liquid water path (LWP) indicates that our proposed method retrieves more accurate LWC products than that from the traditional empirical algorithms.**

***Index Terms*— Liquid water content (LWC), mass absorption attenuation, millimeter-wavelength radar.**

I. Introduction

CLOUDS play a critical role in the Earth energy budget through their albedo effect by reflecting solar radiation back to space and the greenhouse effect by absorbing thermal radiation emitted from the underlying atmosphere and Earth's surface [1], [2], [3], [4], [5], [6]. These cloud radiative processes can change the atmospheric heating rate [7] and modify horizontal and vertical temperature gradients, which will essentially modulate atmospheric circulation, planetary energy transportation, and precipitation distribution [8], [9], [10], [11]. Different types of clouds have distinct cloud radiative effects, which are largely controlled by their macro- and microphysical properties such as height, horizontal extent, optical thickness, droplets phase, and size [12], [13]. Low-level clouds (LLCs) are lower than 2–3 km and cover approximately one-fifth of the Earth's surface [14]. LLCs cool the climate by strongly reflecting solar radiation back to space while emitting comparable amount of longwave radiation as the surface due to their similar temperatures [15], [16], [17]. It is estimated that the cooling effect induced by mere 4% increase in the LLC fraction can compensate the global warming by doubling CO_2 [18]. However, LLC and the associated climate feedback effects are poorly represented by the climate models due to a lack understanding of their microphysical process, leading to the largest source of uncertainty in climate prediction [19], [20], [21]. To improve the representation of LLC in climate model, comprehensive and long-term observations of cloud properties are essential [22], [23], [24]. Liquid water content (LWC) is a vital factor to determine the cloud radiative properties and to parameterize the microphysical process in both general circulation models (GCMs) and cloud resolving models [17], [25], [26]. An accurate estimation of LWC is important to improve the understanding of LLC properties and to improve their representation in climate models.

Various techniques have been developed to retrieve LWC for a series of remote sensing instruments. One of the most widely used instruments is the millimeter-wavelength radar, also known as cloud radar. Benefited by the utilization of short wavelength, cloud radar is sensitive to the presence of cloud droplets and has been recognized as an effective tool to investigate the cloud vertical structures with high temporal and spatial resolutions [27], [28], [29]. The primary radar observational product is radar reflectivity (Z), which is proportional to the six-power of the liquid droplet diameter. Z is commonly applied to retrieve LWC by the following steps: first, the relationship between Z and LWC is proposed as $Z = a\text{LWC}^b$; then, the coefficients in the Z–LWC relationship are derived from aircraft measurements or model simulations

Manuscript received 19 September 2022; revised 1 March 2023 and 20 April 2023; accepted 17 May 2023. Date of publication 22 May 2023; date of current version 6 June 2023. This work was supported in part by the National Natural Science Foundation of China under Grant 42275076, Grant 41875028, and Grant 91937302; in part by the Science and Technology Project of Gansu Province under Grant 22JR5RA446; and in part by the Fundamental Research Funds for the Central Universities under Grant lzujbky-2022-ct06. *(Corresponding author: Jianping Huang.)*

Jinming Ge, Jiajing Du, Zheyu Liang, Jing Su, Qinghao Li, Qingyu Mu, and Jianping Huang are with the Key Laboratory for Semi-Arid Climate Change of the Ministry of Education and the College of Atmospheric Sciences, Lanzhou University, Lanzhou 730000, China (e-mail: hjp@lzu.edu.cn).

Zeen Zhu is with the Environmental and Climate Sciences Department, Brookhaven National Laboratory, Upton, NY 11973 USA.

Qiang Fu is with the Department of Atmospheric Sciences, University of Washington, Seattle, WA 98105 USA.

Digital Object Identifier 10.1109/TGRS.2023.3278735

by assuming a cloud droplet size distribution (DSD) following a lognormal or Gamma distribution [30], [31], [32], [33]. Even though this empirical relationship-based algorithm is widely used, there are several disadvantages that limit its applicability for LWC retrieval [34], [35], [36], [37]. For instance, the derived coefficients are regime-depended and the assumed DSD is affected by the meteorological and aerosols conditions. Thus, the derived Z–LWC relationship is only applicable to a certain location with similar cloud microphysical properties. The mismatch between in situ detection and radar sensing volumes may potentially induce further uncertainties to the constructed empirical relationship. Another noticeable limitation of the algorithm is that it is unable to retrieve the LWC in the presence of drizzling as the large drizzle particles significantly enhance radar reflectivity but contribute little to LWC due to their relatively low concentration. Moreover, the uncertainty of the LWC retrieval is sensitivity to the accuracy of reflectivity measurement and requires absolute radar calibration. However, the calibration for a continuous operating radar system is challenging since the parameters of radar transmitter and receiver system can drift due to changing ambient temperature, pressure, and system components aging [38], [39], [40], [41].

Besides the empirical relationship, other approaches have been developed to retrieve LWC by taking advantage of the microwave attenuation characteristics. Particle scattering efficiency is proportional to the fourth power of its size parameter α (e.g., $\alpha = 2\pi r/\lambda$, where r is the particle radius and λ is the radar wavelength), while the absorbing efficiency is proportional to the first power of α. Cloud droplet scattering can be neglected for a very small α in the Rayleigh approximation by comparing the micrometer-scale cloud particle radius to the millimeter radar wavelength. The amount of the attenuated signal dominated by cloud droplet absorption is therefore proportional to the liquid water mass through the wave propagation path. Thus, the LWC can be directly retrieved if the signal attenuation is estimated at each radar gates [42], [43]. One commonly used approach to estimate the attenuation is to use the dual-wavelength radar observation. In particular, the reflectivity difference (in dBZ) from two radars with different wavelengths, which is called the dual-wavelength ratio (DWR), can be unambiguously determined from observation. The DWR is a direct measure of the attenuation difference in clouds for two wavelengths. Using DWR combined with the theoretical estimated attenuation parameters, the LWC can be directly obtained [42], [43], [44], [45], [46], [47]. The notable advantage of the DWR method is that the algorithm is independence of DSD assumption and can retrieve LWC in the presence of drizzle particles. However, the successfully application of the DWR methods requires strict settings and alignment: the two radars should be placed closely to each other and operate with the same beamwidth and resolution to avoid any mismatch of the cloud observation. These stringent conditions limit the application of DWR algorithm.

In this study, we propose a novel method to retrieve LWC by utilizing the liquid water mass attenuation characteristic, but only with a single-wavelength millimeter cloud radar. The original unattenuated reflectivity (Z_e, i.e., intrinsic reflectivity) is expressed with a few key parameters and a self-consistent relationship between the measured reflectivity (Z_m), the LWC, and the intrinsic reflectivity after attenuation correction is established. A nonlinear least-square regression technique is utilized to optimize these parameters and obtain the LWC. This work is structured as follows. The instruments and datasets used are introduced in Section II. The theoretical basis and the sensitivity analysis of the algorithm are described in Sections III and IV, respectively. In Section V, the algorithm is applied to observational data for different cases and is evaluated using the LWP from microwave radiometer (MWR). The statistical analysis of retrievals applied to one-year observations for LWC and LWP is performed in Sections VI and VII. Summary and conclusions are given in Section VIII.

II. Instrument and Dataset

The data used in this study are collected from the Eastern North Atlantic (ENA) site (39.09° N, 28.02° W) located on the Graciosa Island in the Azores archipelago. ENA observational site is established by the U.S. Department of Energy Atmospheric Radiation Measurement (ARM) since 2015 and provides comprehensive marine boundary layer cloud observations [48], [49], [50]. The observations of 35-GHz Ka-band zenith radar (KAZR), micro-pulse lidar (MPL), Vaisala Laser Ceilometer (CEIL), and the three-channel MWR are used in this study.

Here, we use one-year Active Remote Sensing of Clouds (ARSCL) value-added product from 1 June 2017 to 31 May 2018 to develop and verify the LWC retrieval algorithm. The KAZR records with a 4-s temporal resolution and 30-m vertical resolution. The ARSCL product synthesizes KAZR, MPL, CEIL, and MWR observations and provides the best estimation of reflectivity and cloud base height information [51], [52]. The best estimated reflectivity is the KAZR co-polarized reflectivity of hydrometeor that is filtered from background noise and low-level clutters [51], [52], [53], [54]. The best estimated cloud base height is determined through the backscatter recorded by MPL and CEIL. Cloud top is defined as the height of the highest hydrometeor echo in each continuous radar profile for single- and multiple-layered clouds. Liquid water cloud is selected with radar profiles with cloud top lower than 4 km and cloud base lower than 3 km.

The liquid water path (LWP) of the MWR product (hereafter $\mathrm{LWP_{MWR}}$) with an uncertainty of 20 g $\mathrm{m^{-2}}$ is interpolated into a 4-s resolution to match the radar time resolution. $\mathrm{LWP_{MWR}}$ is used for comparing and validating the retrieved LWP from the proposed algorithm (hereafter $\mathrm{LWP_{Ret}}$) and the traditional empirical algorithm (hereafter $\mathrm{LWP_{Tra}}$). Since the MWR-retrieved LWP is biased when MWR is wet, only the radar profiles with the minimum range of the hydrometeor echo greater than 250 m above ground level are selected in this work.

III. Retrieval Method

For a given cloud DSD, the reflectivity can be well estimated according to the Mie scattering theory, which is called the radar unattenuated reflectivity Z_e. However, the measured radar reflectivity Z_m is a value of the Z_e after attenuation

by the LWC through the transmission path. Based on the principle of radar observation and the radiative transfer theory, an equation relating Z_e, Z_m, and LWC can be constructed to resolve the radar signal attenuation process as propagates in a liquid cloud layer. The details of the algorithm description and application to single- and multiple-layer clouds are elaborated in Sections III-A and III-B, respectively. Equations (1)–(3) are the basic formulas to describe the principles of radar power propagation and its attenuation by cloud liquid droplets. Equations (4)–(7) are the procedure for how to construct the expression of cloud LWC based on the absorption attenuation. Equations (8) and (9) give the error functions established to obtain the optimal parameters. Equations (10) and (11) depict how to distinguish the radar reflectivity attenuation caused by the upper layer cloud water content from that caused by the lower layer cloud for an application to a multiple-layer cloud.

A. Theory of LWC Retrieval Algorithm for Single-Layer Cloud

Because of the absorption of radar power due to the gas and liquid cloud droplets, the radar measured reflectivity (in unit of $\mathrm{mm^6 m^{-3}}$) is smaller than the original unattenuated reflectivity. Thus, the measured reflectivity can be expressed as the unattenuated reflectivity multiplied by the two-way total transmittance in a cloud layer as

$$Z_m(r_i) = Z_e(r_i)\exp\left(-2\times 0.23\int_{r_0}^{r_i} A(s)\mathrm{ds}\right) \tag{1}$$

where r_0 is the radar range at the cloud base, r_i is the ith range from the cloud base, and the cloud top range is denoted as r_T. A is the one-way attenuation coefficient (dB $\mathrm{km^{-1}}$) and can be expressed as (2) when the cloud droplet extinction features are considered under the Rayleigh approximation [55]

$$A = K^*\mathrm{LWC} \tag{2}$$

where K^* is the mass attenuation coefficient in the units of $\mathrm{dB{\cdot}km^{-1}/(g{\cdot}m^{-3})}$, which is a function of the radar wavelength, cloud temperature, and cloud particle phase. Assuming a limited temperature variation in LLC, the coefficient K^* can be treated as a constant for a cloud radar at a given wavelength [56]. By substituting (2) into (1), we have

$$Z_m(r_i) = Z_e(r_i)\exp\left(-0.46K^*\int_{r_0}^{r_i}\mathrm{LWC}(s)\mathrm{ds}\right). \tag{3}$$

According to the physical definitions of the unattenuated reflectivity and LWC, which are proportional to the sixth and the third power of the particle radius, respectively, it is logical to assume an exponential relationship between LWC and Z_e in the form $\mathrm{LWC} = aZ_e^b$. Equation (3) can be further rewritten to a Bernoulli differential equation as (4), which is much easier to perform an integration of the $\mathrm{LWC}(r_i)$ at each radar range [57], the relevant details of which are supplemented in the Appendix

$$\begin{aligned}\frac{\mathrm{dv}}{v^2} &= 0.46abK^*Z_m^b\mathrm{dr}\\ v &= e^{\mathrm{bx}}\\ x &= 0.46K^*\int_{r_0}^{r} aZ_e^b(s)\mathrm{ds}.\end{aligned} \tag{4}$$

By integrating (4) from r_0 to r_i and r_T, the relationship between $\mathrm{LWC}(r_i)$, $Z_m(r_i)$, and $\mathrm{LWC}(r_T)$ can be established as

$$\begin{aligned}\mathrm{LWC}(r_i) &= \frac{Z_m^b(r_i)\mathrm{LWC}(r_T)}{Z_m^b(r_T)+\mathrm{LWC}(r_T)I(r_i,r_T)}\\ I(r_i,r_T) &= \int_{r_i}^{r_T} 0.46bK^*Z_m^b(s)\mathrm{ds}.\end{aligned} \tag{5}$$

Considering the exponential relationship between LWC and Z_e and combining (1), it is straightforward to obtain the expression $\mathrm{LWC}(r_T) = aZ_m^b(r_T)\exp(0.46bK^*\mathrm{LWP})$, where $\mathrm{LWP} = \int_{r_0}^{r_T}\mathrm{LWC}(s)\mathrm{ds}$. Note that there is a parameter $\boldsymbol{a}$ in this expression. To eliminate this parameter on the retrieval uncertainty, we integrate (4) from r_0 to r_T to obtain the equation of $(1/(\exp(0.46bK^*\mathrm{LWP}))) = \mathrm{aI}(r_0,r_T)$ and substitute it to the expression for $\mathrm{LWC}(r_T)$ above. Thus, $\mathrm{LWC}(r_T)$ can be further expressed as

$$\mathrm{LWC}(r_T) = \frac{Z_m^b(r_T)}{I(r_0,r_T)}\left[\exp\left(0.46bK^*\mathrm{LWP}\right)-1\right]. \tag{6}$$

By substituting (6) into (5), one can see that the LWC at any range between r_0 and r_T [i.e., $\mathrm{LWC}(r_i)$] can be expressed as follows, which gives the intrinsic links between the $\mathrm{LWC}(r_i)$, radar reflectivity, and LWP:

$$\mathrm{LWC}(r_i) = \frac{Z_m^b(r_i)\left[\exp(0.46bK^*\mathrm{LWP})-1\right]}{I(r_0,r_T)+\left[\exp(0.46bK^*\mathrm{LWP})-1\right]I(r_i,r_T)}. \tag{7}$$

Here, an assumption is made that $Z_e(r_0) = Z_m(r_0)$ at the cloud base by neglecting the cloud water content absorption in the first 30-m range and other gas absorption below the cloud base. In order to obtain the optimal parameters in (7) for the LWC retrieval of each cloud profile, it is necessary to construct an error function of $F(x)$ as given in (9) between a reconstructed reflectivity Z_{mc} shown in (8) and the radar measured reflectivity Z_m for each height of the cloud profile from cloud base to top, where $c = (1/a)^{(1/b)}$ and x is a vector with three parameters (i.e., $x = [\,b\ \mathrm{LWP}\ c\,]$)

$$Z_{\mathrm{mc}}(r_i) = c(\mathrm{LWC}(r_i))^{\frac{1}{b}}\exp\left(-0.46\int_{r_0}^{r_i}K^*\mathrm{LWC}(s)\mathrm{ds}\right) \tag{8}$$

$$\min_x\|F(x)\|_2^2 = \min_x\sum_i (f_i(x))^2$$

$$F(x) = \begin{bmatrix} f_{r_0}(x)\\ f_{r_1}(x)\\ \vdots\\ f_{r_i}(x)\\ \vdots\\ f_{r_T}(x)\end{bmatrix} = \begin{bmatrix} \mathrm{dBZ_{mc}}(r_0)-\mathrm{dBZ}_m(r_0)\\ \mathrm{dBZ_{mc}}(r_1)-\mathrm{dBZ}_m(r_1)\\ \vdots\\ \mathrm{dBZ_{mc}}(r_i)-\mathrm{dBZ}_m(r_i)\\ \vdots\\ \mathrm{dBZ_{mc}}(r_T)-\mathrm{dBZ}_m(r_T)\end{bmatrix}. \tag{9}$$

The optimal values of $\boldsymbol{b}$, LWP, and $\boldsymbol{c}$, which correspond to the minimization of the error function, can be obtained through achievement of self-consistent process between Z, LWC, and attenuation by using the trust region reflective (TRR) numerical iteration method, which has good performance in solving nonlinear least-square problems [58], [59], [60]. The termination tolerances and initial, upper, and lower boundaries

(LBs) of the parameters are necessary for the TRR method to accelerate iterative convergence and avoid impractical values. Here, the tolerances, including both the minimum changes of variable vector and objective function, are set as 10^{-6} [61], [62], [63], [64], [65]. Since liquid droplets with different sizes contribute differently to the cloud LWC, we classify the clouds into nonprecipitation clouds and cloud with drizzle by setting a radar reflectivity threshold to help speed up the iterative convergence for obtaining the optimal parameters by setting two different initial values. Different reflectivity threshold has been proposed as a threshold to identify drizzle from cloud radar observations in previous studies, among which –15 dBZ suggested by Frisch et al. [66] is the most widely utilized value. Thus, we adopt a threshold of –15 dBZ and set the LB of the x vector as zero to constrain the parameters in the nonnegative range and the initial x vector and upper boundary (UB) as two categories, i.e., the initial x and upper bound for the profile with maximum reflectivity less than –15 dBZ are set as

$$x_0 = \begin{bmatrix} 0.5 & 0.01 & 0.01 \end{bmatrix} \quad \text{and} \quad x_{\mathrm{UB}} = \begin{bmatrix} 1 & 1 & 1 \end{bmatrix}$$

where the initial value of parameter $\boldsymbol{b}$ is set to 0.5 by considering that the reflectivity factor and LWC are proportional to the sixth and third powers of the cloud droplet diameter, respectively. The upper bound of LWP is set to 1 since the cloud LWP does not exceed 1 kg m^{-2} and the upper bound of parameter $\boldsymbol{c}$ is set to 1 referring to the various empirical coefficients proposed in previous studies that the parameter $\boldsymbol{a}$ is usually greater than 1 and the parameter $\boldsymbol{b}$ is less than 1 for the nonprecipitation cloud. Analogously, the initial x and upper bound for the profile with maximum reflectivity no less than this threshold are set as

$$x_0 = \begin{bmatrix} 0.5 & 0.1 & 0.01 \end{bmatrix} \quad \text{and} \quad x_{\mathrm{UB}} = \begin{bmatrix} 1 & 1 & \text{null} \end{bmatrix}$$

(null means that the upper bound cannot be determined), where the LWP initial is set as 0.1 considering that the cloud with drizzle has an abundance of liquid water and setting a larger initial value is beneficial to speed up and accurately obtain the optimal parameters. In addition, if the absolute difference between any element of the optimal vector and the initial bound is less than 10^{-4}, which indicates that the initial x is too close to the local optimum and the iteration process is invalid. Thus, the initial vector should be modified as smaller values (i.e., $x_0 = \begin{bmatrix} 0.01 & 0.01 & 0.01 \end{bmatrix}$) for ensuring the validity of the iteration. The framework of the retrieval method is shown as the form of flowchart in Fig. 1.

According to (8), the reconstructed reflectivity Z_{mc} depends on three parameters (i.e., $\boldsymbol{b}$, $\boldsymbol{c}$, and LWP), and the error between it and the radar measured reflectivity for a range of these parameters can be uniquely calculated. Fig. 2 shows an example of the algorithm in obtaining the optimal parameters and retrieving LWC from one cloud radar observed reflectivity profile at 11:36 UTC on 30 June 2017 at the ENA site. The 3-D diagram in the lower panel of Fig. 2 shows the root-mean-square error (RMSE) between the reconstructed reflectivity and the measured reflectivity varying with the changes of the three parameters for this specific cloud profile, where

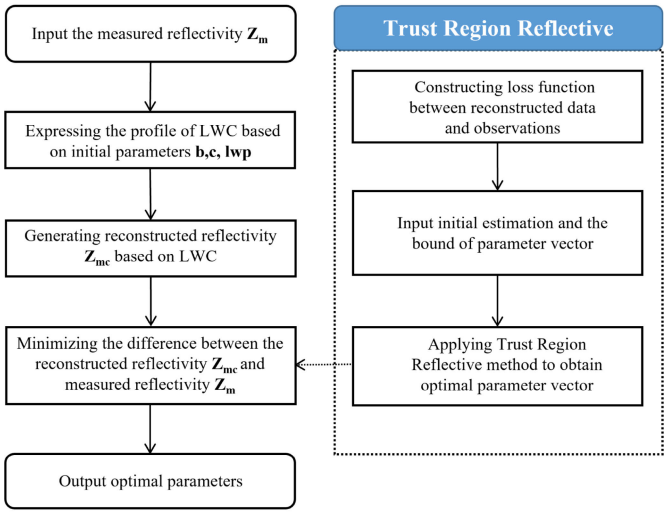

Fig. 1. Flowchart of the retrieval algorithm. (Left) Framework of the overall algorithm. (Right) Details of the TRR algorithm used for obtaining the optimal parameters.

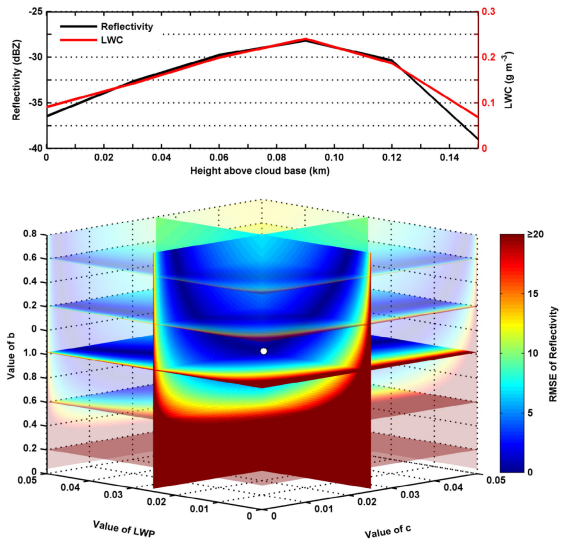

Fig. 2. (Top) Schematic of the retrieval algorithm shown with the vertical profile of radar measured reflectivity (black line) and retrieved LWC (red solid line). (Bottom) RMSE of the reconstructed reflectivity and measured reflectivity versus the three parameters. The optimal parameter value gained by the TRR algorithm is marked by white dot at the intersection of three planes.

the parameters b, c, and LWP ranging from 0 to 1, 0 to 0.05, and 0 to 0.05 g/m^2, respectively. Here, only several 2-D sections are depicted to illustrate how the RMSE changes with the other two parameters when the third one is fixed. For instance, the vertical section parallel with the $\boldsymbol{b}$– $\boldsymbol{c}$ plane at a constant LWP value of 0.05 g/m^2 shows the distribution of the retrieval errors versus the variation of parameters $\boldsymbol{b}$ and $\boldsymbol{c}$, and the horizontal LWP-$\boldsymbol{c}$ plane at the top shows the impact of LWP and $\boldsymbol{c}$ on the error of reflectivity for a given $\boldsymbol{b}$ of 0.9. Ideally, if a proper set of parameters $\boldsymbol{b}$, $\boldsymbol{c}$, and LWP that correspond to the minimum error between the reconstructed and the measured reflectivity can be found, it is possible to accurately calculate the LWC. Note that a dark

blue region exists, where three perpendicular sections with the lowest transparency intersect show the situation that the reconstructed reflectivity is very close to the actual measured reflectivity with small RMSE value. The optimal parameters determined by the TRR algorithm should be located in this dark blue area. Encouragingly, the optimal values of 0.0508, 0.025, and 0.025 g/m^2 for $\boldsymbol{b}$, $\boldsymbol{c}$, and LWP derived from TRR marked as the white dot in Fig. 2 (bottom) are exactly in this region, confirming that the whole retrieval algorithm is reliable. By applying the optimal parameters to (7), the LWC profile is derived and shown as the red solid line in Fig. 2 (top). The LWC distribution tends to increase and then decrease with height that is consistent with the typical features of LWC in nonprecipitation clouds [67].

B. Modification of the Algorithm for Multiple-Layer Clouds

The presence of multiple-layer clouds is common over the ocean, and hence, adjusting the algorithm for the application to the clouds more than one-single layer is necessary. We take a two-layer cloud as an example to illustrate the modification of the retrieval method. In order to accurately obtain the LWC for the upper layer cloud, it is crucial to distinguish the radar reflectivity attenuation caused by its own cloud water content from that caused by the lower layer cloud. The LWC in the lower cloud layer (first layer) is derived following the same steps as the single-layer cloud. Then, the retrieved LWC is used to quantify the attenuation for the upper layer cloud. Again, the gas absorption between the two cloud layers is neglected. The relationship between the intrinsic reflectivity and the attenuated reflectivity for the upper layer cloud can be expressed as

$$Z_m(r_{2i}) = Z_e(r_{2i}) \exp\left(-0.46 \int_0^{r_{2i}} A_{12}(s)\mathrm{ds}\right)$$
$$\int_0^{r_{2i}} A_{12}(s)\mathrm{ds} = \int_{r_{10}}^{r_{1T}} A_1(s)\mathrm{ds} + \int_{r_{20}}^{r_{2i}} A_2(s)\mathrm{ds} \tag{10}$$

where A_{12} is the total one-way attenuation coefficient for the whole cloud layers (i.e., both the lower and upper layer clouds); r_{n0}, r_{nT}, and r_{ni} are the heights of cloud base, cloud top, and the ith range gate, respectively; and A_n is the attenuation coefficient for a cloud layer. The subscript n corresponds to the number of the cloud layer. Considering the attenuation caused by the lower layer cloud, the corrected reflectivity Z'_m of the second cloud layer can be derived from (11), where $A_1 = K^*\mathrm{LWC}_1$

$$Z'_m(r_{2i}) = Z_m(r_{2i}) \exp\left(0.46 \int_{r_{10}}^{r_{1T}} A_1(s)\mathrm{ds}\right). \tag{11}$$

After the correction of the radar reflectivity caused by the lower layer cloud attenuation, the process described in Section III-A is repeated to obtain the optimal parameters for the upper layer cloud based on the initially corrected reflectivity Z'_m. The error function is also modified as the error between the reconstructed corrected reflectivity Z'_{mc} and Z'_m. By applying these three steps, the LWC profile for each layer cloud can be retrieved. For clouds more than two layers, it only needs to sequentially calculate the LWC from the lowest layer to the upper layer and use the LWC in lower layer to perform the radar reflectivity correction for the upper layer.

In reality, large droplets can often fall out of the cloud and become precipitating particles below the cloud base [68]. For this situation, the cloud radar profile can be separated into two layers (i.e., cloud layer and precipitation layer) by combining the ceilometer observations. Similar to the two-layer clouds, it is necessary to calculate the attenuation caused by the precipitating particles under the cloud base in order to correct the radar reflectivity above the cloud base. Since large precipitating particles lead to both strong scattering and absorption in the Mie regime, the attenuation may be no longer proportional to its LWC. Thus, a power law relationship (i.e., $A_d = 1.68Z^{0.9}$, where A_d is the drizzle attenuation coefficient) proposed by Vivekanandan et al. [69] is used to correct the radar reflectivity. After the correction of drizzle attenuation under the cloud base, the LWC above the cloud base can be derived.

IV. Sensitivity Analysis of LWC Retrieval Algorithm

The uncertainties of the retrieval algorithm depend on the accuracy of the radar reflectivity, K^*, the three parameters (i.e., $\boldsymbol{b}$, $\boldsymbol{c}$, and LWP), and the radar reflectivity threshold for classifying clouds with drizzle or not in the algorithm. Here, a sensitivity analysis of the algorithm to these variables is conducted. The uncertainty of the measured reflectivity is expected not to affect the retrieval results since the method relies on the intrinsic absorption amount rather than the absolute accuracy of the reflectivity in this algorithm. K^* relies on cloud temperature, radar wavelength, and cloud phase. For LLC and Ka-band cloud radar, the cloud temperature is the only variable that may affect the retrieval results. Fig. 3(a) shows the bias between the observed reflectivity ($\mathrm{Ref}_{\mathrm{obs}}$) and the retrieved reflectivity ($\mathrm{Ref}_{\mathrm{Ret}}$) by applying the TRR for K^* at different temperatures for the same radar profile as in Fig. 2. The cloud temperature is assumed to vary from 0 °C to 20 °C at an interval of 1 °C. The standard deviation of the reflectivity bias at each range gate height above the cloud base is shown as the shading area in Fig. 3(a), which is less than 2×10^{-8}. In addition, the RMSE of reflectivity for the whole profile is less than 3×10^{-8}, and the solved optimal parameters LWP, b, and c vary within a narrow range of 1 g m^{-2}, 0.1, and 0.001, respectively [Fig. 3(b) and (c)]. This indicates a weak sensitivity of the retrieval to the temperature. Thus, the cloud temperature is assumed to be 0 °C in this study.

The sensitivity of reconstructed reflectivity to b, c, and LWP is shown in Fig. 4. In Fig. 4(a), the LWP is fixed to its optimal value of 0.025 g m^{-2}. b and c will affect the reconstructed reflectivity when the b value is greater than 0.25. For example, given the c value of 0.041 [Fig. 4(a)], a 50% increase of b from 0.508 to 0.762 will cause the RMSE amplified by about three times. The spacing between the adjacent solid lines shows that the RMSE variations caused by a 20% change in the parameter c. It can be seen that the reconstructed reflectivity varies apparently with the change of the c value.

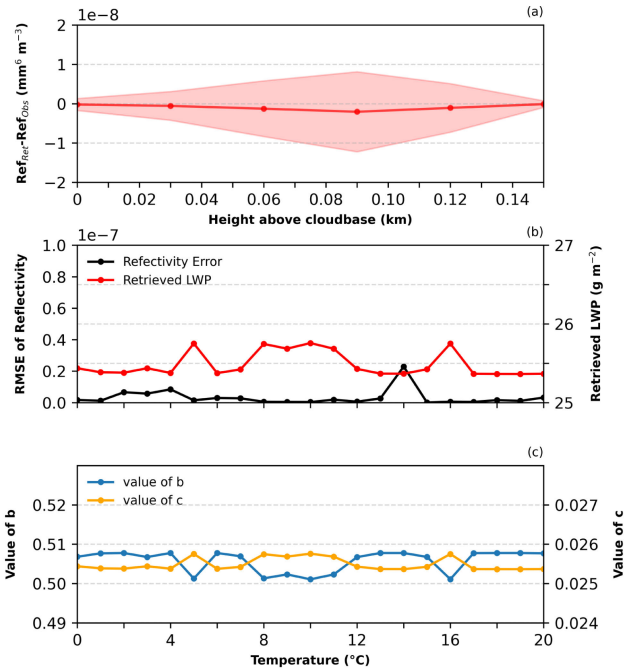

Fig. 3. Sensitivity of the retrieval algorithm to the temperature. (a) Mean error of the reflectivity (red solid line) for each height above the cloud base in the vertical direction with the assumed cloud temperature varying from 0 °C to 20 °C and the shaded region is the standard deviation of the error. (b) RMSE of reflectivity (dark solid line) and retrieved LWP (red solid line) and (c) optimal parameter b (blue solid line) and c (yellow solid line) versus the assumed cloud temperature.

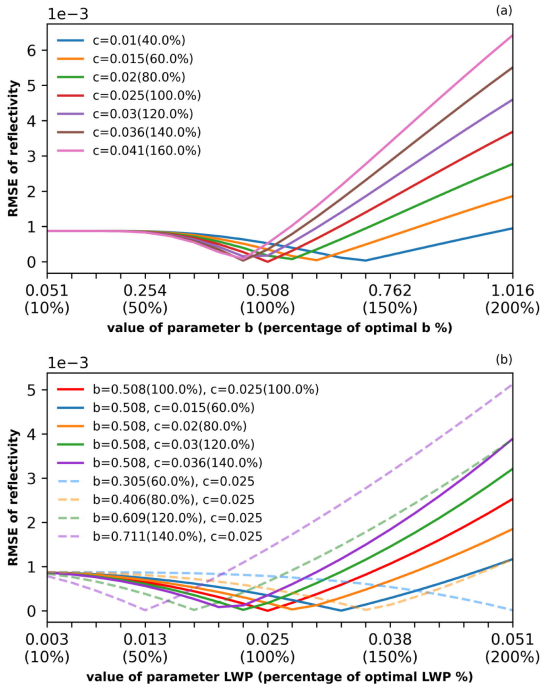

Fig. 4. Sensitivity of the retrieval algorithm to the parameters $\boldsymbol{b}$, $\boldsymbol{c}$, and LWP. RMSE of reflectivity versus (a) parameter $\boldsymbol{b}$ from 0.051 to 1.016 for different $\boldsymbol{c}$ when the LWP is fixed to its optimal value and (b) parameter LWP from 0.003 to 0.051 when $\boldsymbol{b}$ and $\boldsymbol{c}$ are fixed to different values. "RMSE of reflectivity" refers to the RMSE between the reflectivity calculated by applying the varying parameters and the measured reflectivity. The percentages in parentheses give the change of the parameter with respect to the optimal value.

The sensitivity of the algorithm to the different LWP values by fixing b and c values is shown in Fig. 4(b). Generally, the reflectivity is sensitive to the variation of LWP, except that the b value is small (i.e., $b = 0.305$) causing flat variation of RMSE [see the blue dotted line in Fig. 4(b)]. Meanwhile, the retrieval bias is also less sensitive to parameter b when it is close to 0.305 as shown in Fig. 4(a), reflecting that the parameter b plays a key role in the algorithm. In addition, the amplitude of the reflectivity variation is large when the parameters are close to their optimal values, which are the exact turning points of the error, confirming that the optimal parameter values are sensitive to the retrieval error and can be easily found through this error function.

As mentioned in Section III, the –15-dBZ threshold is used to determine the presence of drizzle in the cloud, which was proposed by Frisch et al. [66]. The effect of the different thresholds on the retrieved results is investigated by conducting a sensitivity test with the threshold changing from –14 to –16 dBZ considering the radar reflectivity uncertainty of 1 dB [52]. The results are shown in Table I, where LWC and LWP are the mean values for three different cloud type cases (i.e., single-layer cloud, multiple-layer cloud, and cloud with drizzle below the cloud base) as depicted in Section V and the numbers in parentheses are the percent changes relative to the retrieval values using –15-dBZ threshold. It can be seen that the retrieved results are not sensitive to the different thresholds. The retrieval variations derived from different thresholds are less than 1%. Therefore, a threshold of −15 dBZ is reasonable for determining the presence of drizzle in this retrieval algorithm.

V. Application to Different Cloud Cases

We first apply the algorithm to three cases that are single-layer cloud, two-layer cloud, and drizzling cloud observed at the ENA site. The retrieved results are compared to the MWR-retrieved LWP to evaluate the accuracy of our algorithm. Fig. 5 shows a single-layer boundary cloud on 30 June 2017, occurring from 02:00 to 23:00 UTC. The cloud layer existed around 0.6–0.8 km at the beginning of around 05:00 UTC. After that, both the cloud base and top heights gradually increased to approximately 1.0 and 1.3 km, respectively, and the cloud layer become closed-cell stratocumulus with apparent precipitations at about 20:00 UTC [Fig. 5(a)]. Fig. 5(b) shows the backscatter coefficient of the ceilometer echoing the cloud development as detected from the cloud radar. The cloud base heights derived from the ceilometer are marked as black dots in Fig. 5(a). The attenuation of a few large particles detected by cloud radar under the ceilometer derived cloud base can be neglected in this case since they only occupy few bins in vertical with the reflectivity of less than –15 dBZ. The retrieved LWC from the proposed algorithm is shown in Fig. 5(c). In this shallow marine boundary cloud, the LWC values vary in a small range from 0.03 to 0.29 g m^{-3} most time, except the maximum value of 0.67 g m^{-3} around 19:00 UTC where just before the precipitation. Fig. 5(d) shows the LWP derived from our retrieved LWC and that estimated from the MWR measurements, and the difference between them. It can be seen that the LWP from our retrieval closely follows the MWR observed LWP with a

TABLE I
SENSITIVITY TEST OF RETRIEVAL ALGORITHM TO THE THRESHOLD

Reflectivity Threshold	Single-layer Cloud			Multiple-layer Cloud			Cloud with drizzle below the cloud base		
	LWC ($g \cdot m^{-3}$)	LWP ($g \cdot m^{-2}$)	LWP RMSE	LWC ($g \cdot m^{-3}$)	LWP ($g \cdot m^{-2}$)	LWP RMSE	LWC ($g \cdot m^{-3}$)	LWP ($g \cdot m^{-2}$)	LWP RMSE
-15dBZ	0.15	21.36	15.05	0.15	138.95	37.22	0.25	65.86	22.47
-14dBZ	0.15 (0.000%)	21.36 (0.000%)	15.05 (0.000%)	0.15 (0.13%)	139.15 (0.14%)	37.30 (0.22%)	0.25 (0.39%)	66.28 (0.64%)	22.81 (1.49%)
-16dBZ	0.15 (-0.002%)	21.35 (-0.016%)	15.05 (0.004%)	0.15 (-0.031%)	138.83 (-0.084%)	37.06 (-0.43%)	0.25 (0.11%)	65.79 (-0.12%)	22.49 (0.06%)

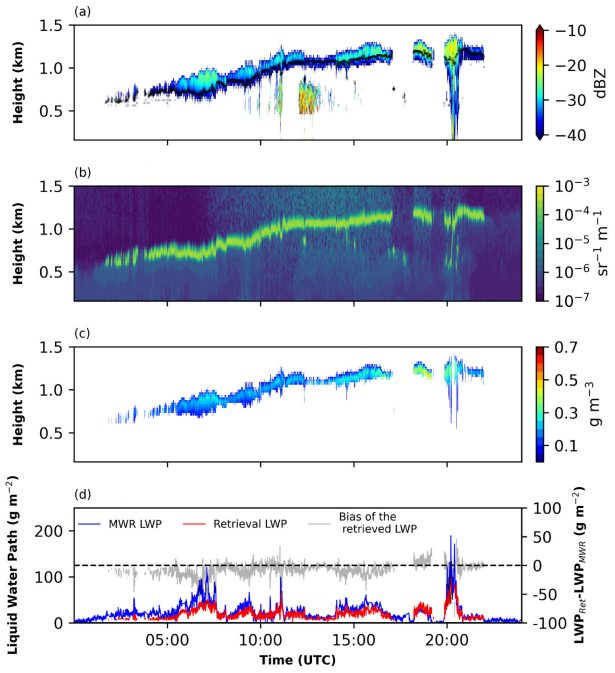

Fig. 5. Case of a single-layer cloud on 30 June 2017. (a) Time–height profiles of the KAZR best estimated reflectivity and the best estimated cloud base marked by the black dots. (b) Time–height profiles of the ceilometer backscatter. (c) Time–height profiles of the retrieved LWC. (d) Left ordinate: the retrieved LWP (red line) and observed LWP from the MWR (blue solid line). Right ordinate: error of the retrieval algorithm (gray solid line).

mean bias (MB) of only –8.6 g m^{-2} and a standard deviation of 12.4 gm^{-2}. Note that some large differences around 20:00 UTC might be explained by the precipitation, which will induce an overestimation of LWP by MWR. Overall, this good agreement suggests that our method is capable of accurately retrieving LWC for this single-layer cloud.

Fig. 6 shows a two-layer cloud case of 30 April 2017 observed from 09:00 to 09:24 UTC. The first and second cloud layers appear at about 0.5 and 1.5 km, respectively. The cloud base height of the first layer is determined by the best estimated cloud-base marked with black dots [Fig. 6(a)] and the second-layer base is estimated from the lowest radar signal echoes. A few range bins below the cloud base with weak reflectivity at about 09:04 and 09:12 UTC may be wrongly identified as cloud by the radar cloud mask method, which is neglected in this study. The LWCs of the first-layer cloud are obtained by applying the retrieval algorithm for a single-layer cloud [Fig. 6(b)]. Fig. 6(c) shows that the initially corrected reflectivity of the second layer with only the first-layer attenuation is considered. It is obvious that the differences between the initially corrected and measured reflectivity [see black solid line in Fig. 6(c)] have a similar variation with the maximum reflectivity from the first layer. This confirms that the lower layer cloud has a significant attenuation effect on the upper layer cloud. Based on the corrected reflectivity, the LWC profiles for upper layer cloud are retrieved, ranging from 0.01 to 0.34 g m^{-3} [Fig. 6(d)]. Based on the cloud LWC, the attenuation coefficient related to the liquid cloud particle's absorption for different cloud layer can be quantified and the difference between the corrected and measured reflectivity are shown in Fig. 6(e), where the corrected reflectivity is calculated by quantifying the absorption attenuation of the two cloud layers. The attenuation strength is less than 0.74 dB. Huang et al. [70] showed that the attenuation by water cloud is generally within 1 dB. The comparisons of LWP_{Ret} with LWP_{MWR} [Fig. 6(f)] show a good agreement with an MB and a standard deviation of 19.38 and 31.78 g m^{-2}, respectively. Moreover, we have noticed an apparent difference between LWP_{MWR} and LWP_{Ret} in the preceding segment of the upper cloud layer in Fig. 6, where large reflectivity appears. We would explain this discrepancy by the inhomogeneous cloud distribution and the difference between MWR and radar field of view. The upper cloud layer with relatively higher reflectivity has a more significant discontinuous distribution. Since the beamwidth of MWR is larger than that of cloud radar, inducing coarser MSU sampling resolution as the distance between cloud and remote sensor increases. Thus, these turbulent clouds with strong size and number concentration fluctuations may not be well resolved in space by the MWR.

Fig. 7 shows a single cloud layer with drizzle falling below cloud base observed on 10 September 2017 from 08:00 to 20:00 UTC. Similar to Fig. 5, the black dots shown in Fig. 7(a) are the best estimated cloud base detected by the CEIL. The radar range bins below the cloud base with maximum reflectivity greater than –15 dBZ are regarded as drizzle particles. Using the algorithm described in Section III-B, the retrieved LWP above the cloud base is shown by the red

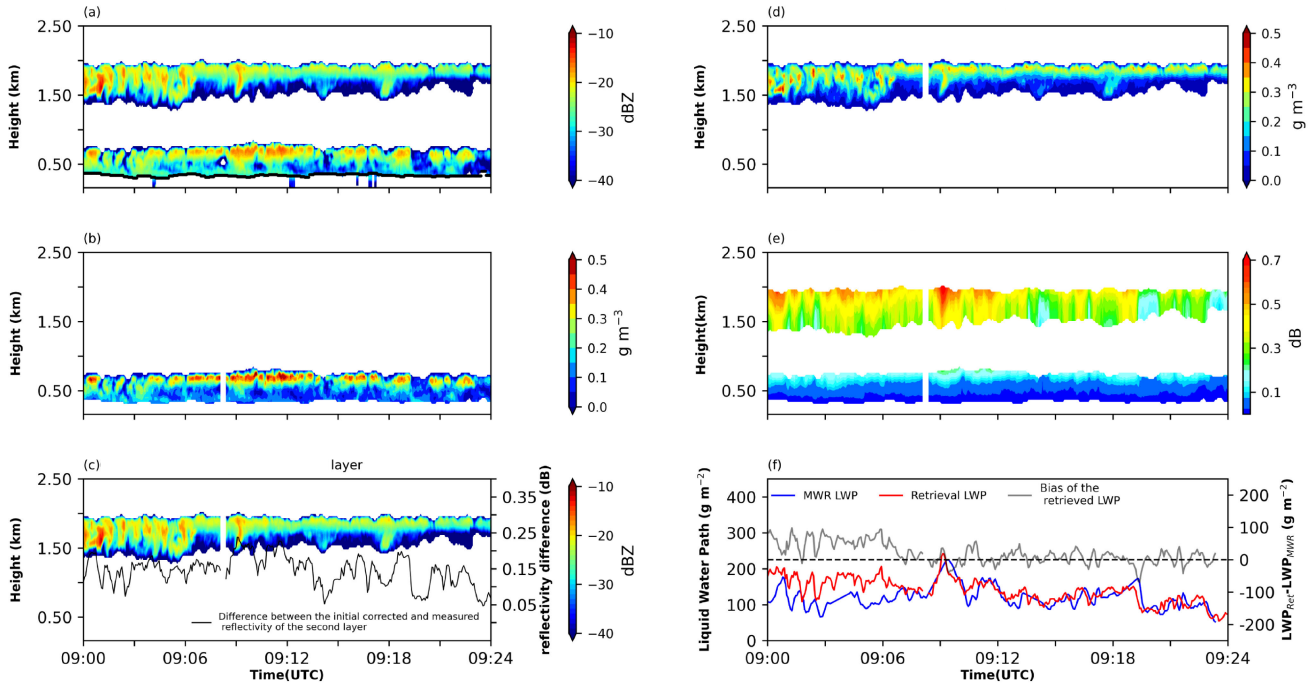

Fig. 6. Case of the double-layer cloud on 30 April 2017. (a) Time–height profiles of the KAZR best estimated reflectivity and the best estimated cloud base marked by the black dots. (b) Time–height profiles of the first-layer cloud retrieved LWC. (c) Time–height profiles of the initial corrected reflectivity for second-layer cloud based on the attenuation due to the absorption of the first-layer cloud and the difference between the corrected and uncorrected reflectivity for each profile (black solid line in the right ordinate). (d) Time–height profiles of the second-layer retrieved LWC. (e) Difference between the unattenuated and measured reflectivity of the first-layer cloud and second-layer cloud. (f) Left ordinate: comparison of the retrieved LWP (red solid line) and the LWP interpolated to the 4-s temporal resolution with the MWR (blue solid line). Right ordinate: error of the retrieval algorithm (gray solid line).

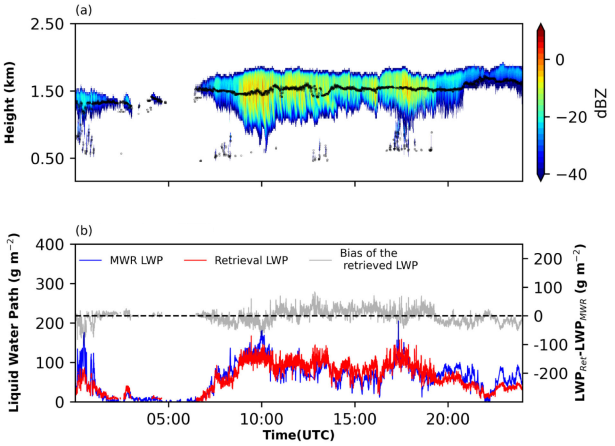

Fig. 7. Case of the cloud with drizzle below the cloud base on 10 September 2017. The description of the graph is the same as Fig. 5. (a) Time–height profiles of the KAZR best estimated reflectivity and the best estimated cloud base marked by the black dots. (b) Left ordinate: comparison of the retrieved LWP (red line) and the LWP interpolated to the 4-s temporal resolution with the MWR (blue solid line). Right ordinate: error of the retrieval algorithm (gray solid line).

solid line in Fig. 7(b), which also has good agreement with LWP_{MWR} with the MB only about –1.30 g m^{-2} in a small standard error of a 22.28 g m^{-2} bias.

VI. Uncertainty Analysis for Retrieved LWC

The uncertainty analysis of the retrieved LWC is performed before we use the method to retrieve LWC from a one-year radar observation. Since the mathematical expressions of our retrieval algorithm have a highly nonlinear nature, it is difficult to quantify the uncertainty directly through the equations. Therefore, we estimate the LWC uncertainty by comparing the retrieved LWC with the LWC provided by the in situ instruments on board the aircraft during the same period at the ENA site.

The ARM Aerial Facility (AAF) Gulfstream-1 (G1) aircraft conducted two intensive observations with 1-s temporal resolution from 21 June to 20 July, 2017 and 15 January to 18 February, 2018, which flew 20 and 19 missions during the summer and winter intensive observation periods (IOPs), respectively [49]. The instruments providing cloud LWC products on board the G1 aircraft include the water content meter (WCM), the cloud volume precipitation spectrometer (CAPS), and the particulate volume monitor (PVM) [71]. We compared the retrieved LWC with four different LWC products provided by the in situ data within 10 km around the ENA site during the entire summer and winter IOPs, as shown in Fig. 8. The in situ data where the altitude is between the radar detected cloud base and top is selected and the retrieved LWC over the three radar bins closest to the aircraft observation height is averaged for comparison. Fig. 8 shows that the retrieved LWC (0.2 ± 0.087 g m^{-3}) is in reasonably good agreement with the LWC provided by the four instruments, i.e., WCM-083 (0.13 ± 0.14 g m^{-3}), WCM-021 (0.10 ± 0.087 g m^{-3}), CAPS (0.10 ± 0.12g m^{-3}), and PVM-100 (0.11 ± 0.1 g m^{-3}). The MBs of the retrieved LWC are 0.073, 0.10, 0.10, and 0.11 g m^{-3}. Taking the in situ

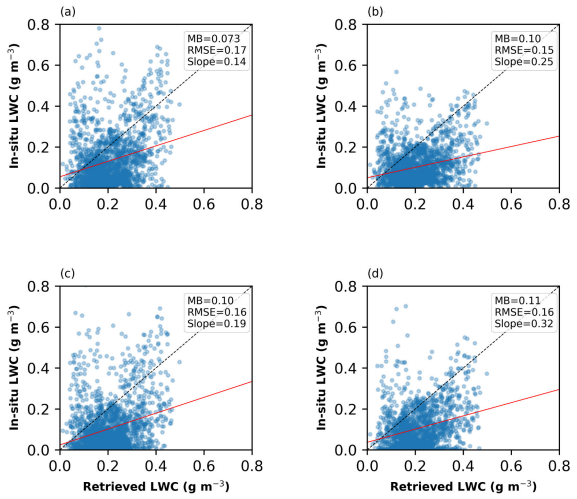

Fig. 8. Comparison of the retrieved LWC with (a) WCM-083, (b)WCM-021, (c) CAPS-Hotwire, and (d) PVM-100 provided by in situ measurements on board of G1 aircraft during the entire ACE-ENA field campaign. The "MB," "RMSE," and "Slope" in the text box at the upper right corner of each subgraph represent the MB between the retrieved and in situ LWC, RMSE, and the slope of the red solid line obtained by fitting the scatter points.

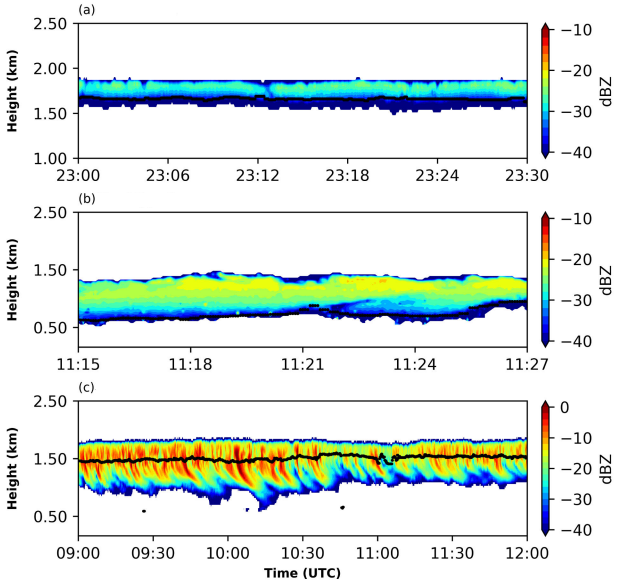

Fig. 9. Schematic of the three cloud types. (a) Cloud type 1 is the single-layer cloud with cloud thickness less than 500 m. (b) Cloud type 2 is the single-layer cloud with cloud thickness not less than 500 m. (c) Cloud type 3 is the cloud with drizzle below the base. The heights of cloud base are marked by dark dots.

data as the true value, the RMSE between retrieved LWC and in situ observations is around 0.15 g m^{-3} for all the four different LWC products. The bias is also affected by the fact that the aircraft and the ground-based observation cannot be completely matched in time and space, as well as by the accuracy of the in situ data itself, which has an uncertainty of 5%–20% for instruments aboard on G1 aircraft.

Three different cloud types, as shown by a schematic in Fig. 9, are considered. The clouds without drizzling below the base are divided into shallow cloud with a thickness of less than 500 m, i.e., cloud type 1 [see an example in Fig. 9(a)], and thick cloud with the depth of more than 500 m, i.e., cloud type 2 [Fig. 9(b)]. Clouds with large drizzling particles below the cloud base are treated as precipitating cloud, i.e., cloud type 3 [Fig. 9(c)].

Since there is no significant difference between the LWC products provided by the four instruments aboard the G1 aircraft, we choose WCM_083 LWC product to further compare with the LWC from our algorithm (LWC_{Ret}) and from the traditional empirical Z–LWC method (LWC_{Tra}), as shown in Fig. 10. For the first cloud type, the mean absolute error (MAE) and RMSE of LWC_{Ret} are smaller than those of LWC_{Tra} (i.e., 0.012 versus 0.13 g m^{-3} and 0.15 versus 0.16 g m^{-3}, respectively), despite the fact that the LWC_{Ret} is similar to the LWC_{Tra} compared with the in situ data. Furthermore, for the second and third cloud types, it is evident that LWC_{Ret} is closer to the aircraft observations than LWC_{Tra} with smaller MAE (0.094 versus 0.17 g m^{-3} for cloud type 2 and 0.16 versus 0.26 g m^{-3} for cloud type 3) and RMSE (0.13 versus 0.22 g m^{-3} for cloud type 2 and 0.22 versus 0.31 g m^{-3} for cloud type 3). Particularly for cloud type 3, which involves large particles, the LWC retrieval bias from our algorithm is effectively reduced compared with the traditional empirical method, which obviously overestimates the LWC. Furthermore, the cumulative distribution functions (CDFs) of the LWC fractional error of our algorithm for the three distinct cloud types (the third row in Fig. 10) are all on the left side of the empirical algorithm, confirming that the error of this new algorithm is smaller than that of the traditional empirical algorithm.

VII. Statistical Analysis for Different Cloud Types From One-Year Data

One-year data from June 2017 to May 2018, including nearly 2 million nonprecipitation profiles, are used to evaluate our LWC retrieval algorithms against the MWR obtained LWP. The LWC from other empirical methods is also derived for comparison.

Fig. 11 shows the LWP retrieved from our algorithm (the top row) and that from the traditional empirical Z–LWC method (the middle row) versus the LWP measured by the MWR. Here, the traditional empirical equations of $LWC = 4.564Z^{0.5}$ [30], $LWC = 0.457Z^{0.19}$ [31], and $LWC = 0.258Z^{0.633}$ [72] are applied to all cloud types for radar profiles with reflectivity lower than –15 dBZ, between −15 and 5 dBZ, and greater than 5 dBZ, respectively. The accuracy of each algorithm for different cloud types was evaluated via the MAE, RMSE, and correlation coefficient (R). For the first cloud type, the MAE and RMSE of the LWP_{Ret} are 16.7 and 27.2 g m^{-2}, which are smaller than those of the LWP_{Tra}. The correlation coefficient between the above two algorithms with the LWP_{MWR} is similar (0.66 versus 0.65). It is worth noting that the CDF of the LWP fractional error of our algorithm is located to the left of the empirical algorithm [Fig. 11(c3)], confirming that the error in our algorithm is smaller than that caused by the empirical algorithm. Taking the CDF equal to 0.5 in Fig. 11(c3) as an example, the corresponding LWP fractional error is 37.6% for our method and 45.6% for the empirical approach, that is, the LWP fractional error is less than 37.6% for 50% of all the profiles if using the

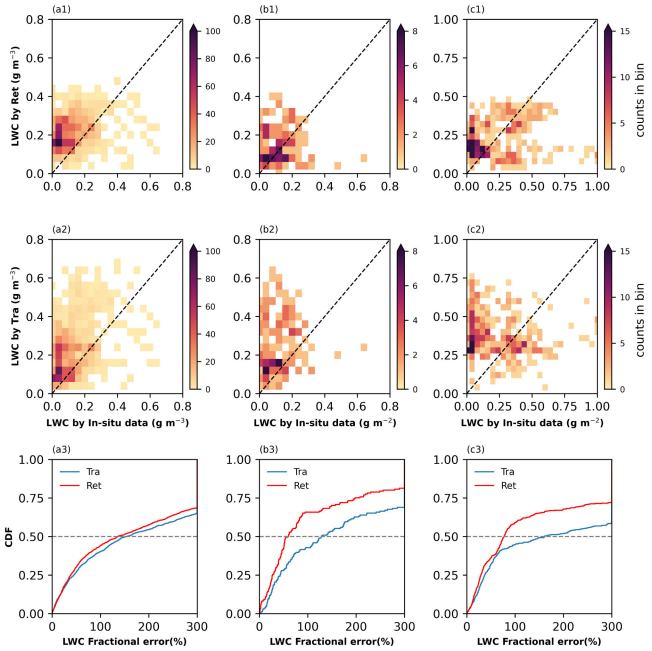

Fig. 10. Evaluation of various retrieval algorithms for (a1)–(a3) cloud type 1, (b1)–(b3) cloud type 2, and (c1)–(c3) cloud type 3, with (top) LWC retrieved by the algorithm in this study and (middle) LWC retrieved by the traditional empirical Z–LWC relationship versus the LWC provided by the WCM on board the G1 aircraft during the entire summer and winter IOPs (the black dashed line represents the same retrieved and in situ LWC). The CDF of the LWC fractional error for the algorithm in this study (blue solid line) and the traditional method (red solid line) are shown in the bottom. The gray dashed line represents that the CDF is equal to 0.5.

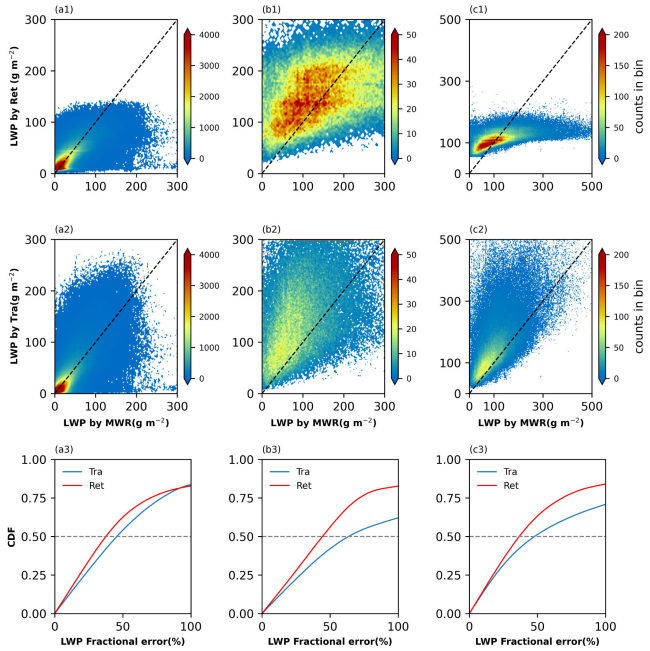

Fig. 11. Evaluation of various retrieval algorithms based on one-year data for (a1)–(a3) cloud type 1, (b1)–(b3) cloud type 2, and (c1)–(c3) cloud type 3, with (top) LWP retrieved by the algorithm in this study and (middle) LWP retrieved by the traditional empirical Z–LWC relationship versus the LWP from the MWR (the black dashed line represents the same retrieved and MWR LWP). (Bottom) CDF of the LWP fractional error for the algorithm in this study (blue solid line) and the traditional method (red solid line). The gray dashed line represents that the CDF is equal to 0.5.

algorithm in this study, while it is 45.6% for the empirical algorithm.

Both cloud types 2 and 3 (see the middle and right columns in Fig. 11) also show that $\mathrm{LWP_{Ret}}$ is closer to the $\mathrm{LWP_{MWR}}$ than $\mathrm{LWP_{Tra}}$ with smaller MAE and RMSE although the correlation coefficient between $\mathrm{LWP_{Ret}}$ and $\mathrm{LWP_{MWR}}$ is smaller for cloud type 3. The CDFs of the two retrieval algorithms have obvious deviations in the horizontal direction, confirming that our LWP retrieval is effectively improved. The $\mathrm{LWP_{Ret}}$ is less than the $\mathrm{LWP_{MWR}}$ when the LWP is greater than 300 g $\mathrm{m^{-2}}$ for cloud type 3, which can be partly attributed to that only the liquid water above the cloud base is retrieved, while the $\mathrm{LWP_{MWR}}$ includes the precipitation water below the cloud. The $\mathrm{LWP_{Tra}}$ is generally larger than $\mathrm{LWP_{MWR}}$, indicating that the LWP obtained by the traditional empirical algorithm is overestimated.

Fig. 12 shows the LWC vertical profiles retrieved from different algorithms for the three cloud types. The equation $\mathrm{LWC}(i) = (\mathrm{LWP}\cdot Z(i)^{(1/2)})/(\sum_{j=1}^{m} \Delta z(j) Z(j)^{(1/2)})$ from [34] is applied in obtaining LWC based on $\mathrm{LWP_{MWR}}$ observation. The height above the cloud base is normalized for a comparison of clouds with different thicknesses. For cloud type 1 with small thickness and low reflectivity, the LWCs retrieved from the three different algorithms are quite similar. For cloud type 2, the LWCs from the empirical algorithm are overestimated compared with the $\mathrm{LWC_{MWR}}$, while $\mathrm{LWC_{Ret}}$ are much close to the MWR retrievals. The LWC distribution of cloud type 3 is similar to that of cloud type 2, with $\mathrm{LWC_{Tra}}$ larger than both $\mathrm{LWC_{MWR}}$ and $\mathrm{LWC_{Ret}}$.

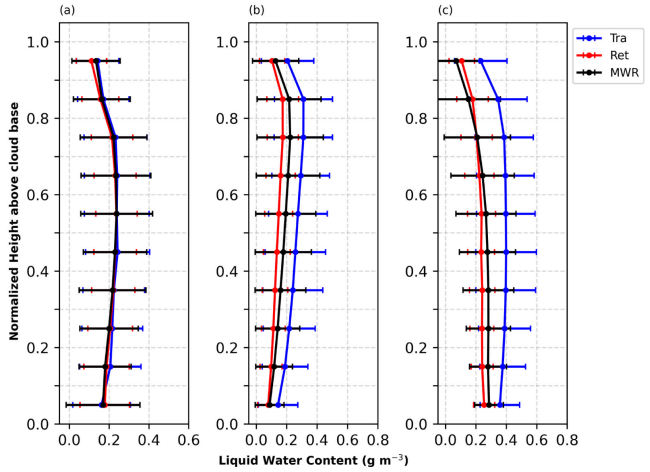

Fig. 12. Profiles of LWC for (a) cloud type 1, (b) cloud type 2, and (c) cloud type 3 versus the normalized height above cloud base (i.e., the ratio of each bin height from the cloud base to the cloud thickness) using the traditional empirical Z–LWC relationship (blue), the algorithm in this study (red), and the method based on the LWP from MWR (black). The solid line is the mean of the LWC and the error bar is the standard deviation of each bin.

Fig. 13 shows the frequency distribution of the derived parameters $\boldsymbol{a}$ and $\boldsymbol{b}$ from our algorithm for the three cloud types. $\boldsymbol{a}$ is calculated from $\boldsymbol{c}$ according to $a = 1/c^b$. For the shallow clouds, the parameter $\boldsymbol{b}$ is concentrated around 0.5 and the parameter $\boldsymbol{a}$ is distributed in a wide range from 3 to 10. Table II provides $\boldsymbol{a}$ and $\boldsymbol{b}$ from previous studies for $\mathrm{LWC} = aZ^b$ [30], [32], [56], [73], [74], [75], [76], [77]. It is encouraging that the distribution range of the parameters obtained in this study is in good agreement with those from

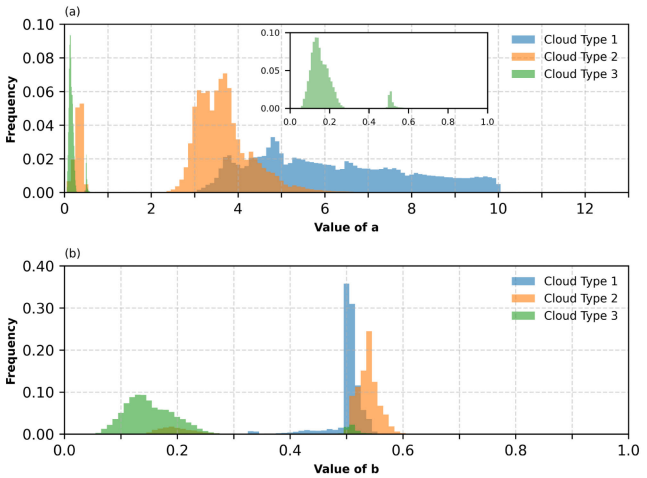

Fig. 13. Frequency histogram of (a) parameter $\boldsymbol{a}$ and (b) parameter $\boldsymbol{b}$ for cloud type 1 (blue bar), cloud type 2 (orange bar), and cloud type 3 (green bar). (Top) Subplot shows the frequency distribution of the parameter $\boldsymbol{a}$ for cloud type 3.

TABLE II

LIST OF COEFFICIENTS PROPOSED IN EARLIER LITERATURE FOR THE EQUATION OF LWC $= aZ^b$ (WHERE THE UNITS OF LWC AND Z ARE G M^{-3} AND MM^{-6} M^3)

a	b	Reference	Cloud Properties
4.564	0.50	Atlas [30]	liquid water cloud
9.27	0.64	Fox and Illingworth [32]	stratocumulus cloud
6.34	0.56	Liao and Sassen [72]	cumulus and stratocumulus clouds
9.65	0.62	Pujol [73]	warm cloud
14.54	0.76	Sauvageot and Omar [74]	warm non-precipitating cumulus and stratocumulus clouds
2.14	0.70	Vivekanandan [75]	non-precipitating cloud
10.29	0.75	Wang and Geerts [76]	drizzle-free stratus

previous studies. For clouds with drizzle below the cloud, the optimal $\boldsymbol{a}$ and $\boldsymbol{b}$ range from 0.1 to 0.8 and from 0.1 to 0.3, respectively. These values are consistent with the coefficients in LWC $= 0.457Z^{0.19}$ in [31]. For the thick clouds, there are two peaks that exist for parameters $\boldsymbol{a}$ and $\boldsymbol{b}$. The distribution of $\boldsymbol{a}$ is centered at 3.7 for one and closed to 0.3 for the other. Correspondingly, $\boldsymbol{b}$ is centered at 0.2 and 0.55. These values have good consistency with the coefficients by previous studies [31] and partially overlap with the parameter distribution interval of cloud type 3.

Fig. 14 shows the derived **a** and $\boldsymbol{b}$ versus the maximum reflectivity for cloud type 2. It can be seen that the profiles with the maximum reflectivity higher than –15 dBZ correspond to the modes with small $\boldsymbol{a}$ and $\boldsymbol{b}$, as for cloud type 3. Therefore, the bimodal distribution of the parameters for cloud type 2 may be attributed to the fact that some cloud profiles containing a few large particles have similar $\boldsymbol{a}$ and $\boldsymbol{b}$ to cloud type 3, while the profiles dominated by relatively smaller particles have partially overlapping regions with cloud type 1. The fact that the retrieved $\boldsymbol{a}$ and $\boldsymbol{b}$ are uniquely determined for each profile but are widely distributed for different cloud profiles illustrates the advantage of our retrieval algorithm over the empirical approach that employs the fixed coefficients

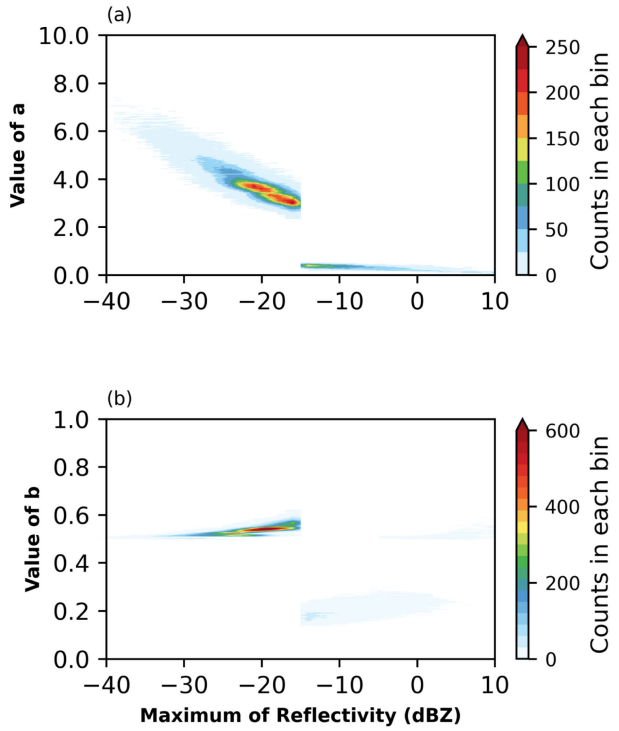

Fig. 14. Relationship between retrieved (a) parameter a and (b) parameter b for cloud type 2 versus the maximum reflectivity.

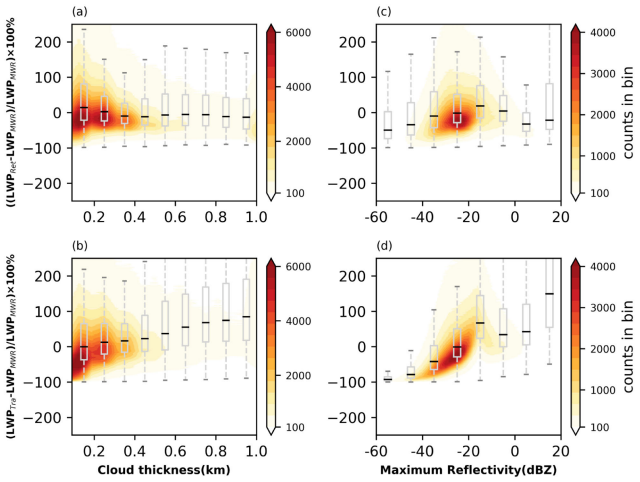

Fig. 15. Retrieved error influenced by cloud layer thickness and maximum reflectivity. Counts of LWP error retrieved by (a) algorithm in this study and (b) traditional method within bins of cloud thickness. The bin width is 0.1 km in the horizontal direction. (c) and (d) are similar as (a) and (b) respectively, with the distinction that the horizontal direction of (c) and (d) is the maximum reflectivity of cloud profile and the bin width is set to 10-dBZ. The gray boxplot is the LWP error distribution within each bin of cloud thickness and maximum reflectivity. The dark solid line in boxplots is the median value in each bin.

provided by the fitting of abundant observation data for all profiles in the traditional empirical relationship.

Since the cloud thickness and the particle size have clear influences on the parameters a and b that directly determine the retrieval uncertainty, we further examine the relative errors in $\mathrm{LWP_{Ret}}$ and $\mathrm{LWP_{Tra}}$ under different cloud thicknesses and maximum reflectivity conditions, as shown in Fig. 15. The shading area filled with different colors represents the samples within each 2% error bin of LWP for vertical coordinate and

0.05 km and 2 dBZ intervals for the cloud thickness and the maximum reflectivity in horizontal coordinate, respectively. The gray boxes show the relative errors at the median and the four percentiles for each 0.1-km interval of cloud thickness and 10-dBZ interval of maximum reflectivity. The error from the traditional empirical method increases with the cloud thickness and reflectivity, which confirms that the exponential relationship will lead to significant overestimations of LWC for clouds with large particles. On the other hand, the error from our algorithm does not have any obvious changes in the cloud thickness and maximum reflectivity, indicating that this algorithm is not affected by large particles.

VIII. Conclusion

In this study, we proposed an algorithm to retrieve the LWC for single-wavelength millimeter cloud radar by constructing a self-consistent function between the unattended reflectivity, measured reflectivity, LWC, and attenuation. It is based on the radiative transfer where the attenuation caused by the cloud droplet absorption is proportional to the LWC under the Rayleigh approximation. The retrieval algorithm is free of cloud particle size distribution assumptions and radar attenuation corrections, which reduces the LWC overestimation of the traditional empirical method when there are large particles in the cloud. It can be applied to both single-layer and multilayer nonprecipitation clouds as well as precipitation clouds with drizzle below the base.

The algorithm is evaluated using one-year Ka-band millimeter-wave radar, MWR observations, and aircraft in situ measurements during summer IOPs at the ENA site. It is demonstrated that the absorption coefficient dependence on the cloud temperature has little impact on the retrieval. By examining the algorithm for different cloud types according to the LWP, the vertical structure of LWC, and the distribution of the derived optimal parameters, we show that our retrieved LWC is in reasonably good agreement with the LWC provided by in situ instruments on board the G1 aircraft during the same period and the retrieved LWP is more consistent with the LWP from the MWR than the LWP from the traditional empirical algorithm. The retrieved error of the new algorithm has little dependence on cloud thickness and radar reflectivity, which is an important improvement to the traditional empirical algorithm that shows large overestimations for thick clouds and large-sized particles with high reflectivity. Furthermore, the parameters/coefficients used in the empirical approaches are in the range of the retrieved ones, but the parameters in the new algorithm are uniquely determined for each radar profile, which is a significant advantage for reducing the error caused by using the fixed coefficients in the traditional empirical algorithm. Considering that this algorithm is based on the detection principle of millimeter-wave radar, it can be modified to be applied to spaceborne single-band millimeter-wave radar to obtain global LWC. However, radar in space observes in a top-down way. It could be challenging to quantify the contribution of ice cloud overlying LLC to the attenuation for further investigate, although most marine LLCs usually form under large-scale downward motion without too much ice clouds above them.

In conclusion, unlike previous method based on empirical relationships, our algorithm starts from the radiative transfer theory and considers the absorption features in the Rayleigh regime to establish a self-consistent relationship among LWC, absorption attenuation, and radar reflectivity. The major limitation of the algorithm is that it requires cloud thickness being greater than three radar bins and it is only valid for cloud droplets with particle sizes compared to millimeter wavelengths satisfying the Rayleigh approximation. The most advantage of this new algorithm is that it leverages the absorption signal instead of correcting it and thus is not affected by the presence of a small amount of drizzle with large particle sizes in the cloud. The method can significantly reduce the large uncertainty in the conventional LWC estimation and is applicable to single-wavelength millimeter cloud radar for cloud LWC retrieval, including the spaceborne radar.

Appendix

The parameters K^*, r_0, and r in (4) represent the mass attenuation coefficient, the radar range at the cloud base, and the range between the cloud base and the cloud top, respectively. Equation (4) is derived from (1) to (3) in this article, and the details of the derivation process are given as follows.

According to (3), the relationship between the unattenuated and measured reflectivity can be rewritten as

$$aZ_e^b(r_i) = aZ_m^b(r_i)e^{0.46bK^*\int_{r_0}^{r_i} aZ_e^b(s)\mathrm{ds}}. \tag{A1}$$

Assuming that

$$x = 0.46K^*\int_{r_0}^{r_i} aZ_e^b(s)\mathrm{ds} \tag{A2}$$

and

$$v = e^{\mathrm{bx}}. \tag{A3}$$

Based on (A2) and (A3), the following differential equations can be gained:

$$\begin{aligned} dx &= 0.46K^*aZ_e^b(r)\mathrm{dr} \\ \mathrm{dv} &= \mathrm{bvdx}. \end{aligned} \tag{A4}$$

Thus, Z_e can be expressed as

$$aZ_e^b(r) = \frac{1}{0.46K^*}\frac{\mathrm{dx}}{\mathrm{dr}} = \frac{1}{0.46K^*}\frac{\mathrm{dv}}{\mathrm{bvdr}}. \tag{A5}$$

By combining (A1) and (A5), we can obtain the formulas as

$$\frac{1}{0.46K^*}\frac{\mathrm{dv}}{\mathrm{bvdr}} = aZ_m^b v. \tag{A6}$$

Namely, from (A6), (A7) in this article is established as

$$\frac{\mathrm{dv}}{v^2} = 0.46\mathrm{ab}K^*Z_m^b\mathrm{dr}. \tag{A7}$$

Acknowledgment

The authors would like to thank the ARM for supporting the ground-based data and aircraft in situ data used in this study (www.arm.gov).

REFERENCES

[1] R. D. Cess et al., "Interpretation of cloud-climate feedback as produced by 14 atmospheric general circulation models," *Science*, vol. 245, no. 4917, pp. 513–516, Aug. 1989, doi: 10.1126/science.245.4917.513.

[2] Q. Fu, M. Baker, and D. L. Hartmann, "Tropical cirrus and water vapor: An effective Earth infrared iris feedback?" *Atmos. Chem. Phys.*, vol. 2, no. 1, pp. 31–37, Jan. 2002.

[3] D. L. Hartmann, M. E. Ockert-Bell, and M. L. Michelsen, "The effect of cloud type on Earth's energy balance: Global analysis," *J. Climate*, vol. 5, no. 11, pp. 1281–1304, Nov. 1992, doi: 10.1175/1520-0442(1992)005<1281:TEOCTO>2.0.CO;2.

[4] H. Jianping, W. Yujie, W. Tianhe, and Y. Yuhong, "Dusty cloud radiative forcing derived from satellite data for middle latitude regions of East Asia," *Prog. Natural Sci.*, vol. 16, no. 10, pp. 1084–1089, Oct. 2006.

[5] V. Ramanathan et al., "Cloud-radiative forcing and climate: Results from the Earth radiation budget experiment," *Science*, vol. 243, no. 4887, pp. 57–63, Jan. 1989, doi: 10.1126/science.243.4887.57.

[6] C. Zhou, M. D. Zelinka, and S. A. Klein, "Impact of decadal cloud variations on the Earth's energy budget," *Nature Geosci.*, vol. 9, no. 12, pp. 871–874, Oct. 2016, doi: 10.1038/ngeo2828.

[7] Q. Fu, K. N. Liou, M. C. Cribb, T. P. Charlock, and A. Grossman, "Multiple scattering parameterization in thermal infrared radiative transfer," *J. Atmos. Sci.*, vol. 54, no. 24, pp. 2799–2812, Dec. 1997, doi: 10.1175/1520-0469(1997)054<2799:MSPITI>2.0.CO;2.

[8] S. Bony et al., "Clouds, circulation and climate sensitivity," *Nature Geosci.*, vol. 8, no. 4, pp. 261–268, Mar. 2015.

[9] R. P. Pearce, *Meteorology at the Millennium*. London, U.K.: Academic, 2002.

[10] S. C. Sherwood, S. Bony, and J.-L. Dufresne, "Spread in model climate sensitivity traced to atmospheric convective mixing," *Nature*, vol. 505, no. 7481, pp. 37–42, Jan. 2014.

[11] A. Voigt, N. Albern, and G. Papavasileiou, "The atmospheric pathway of the cloud-radiative impact on the circulation response to global warming: Important and uncertain," *J. Climate*, vol. 32, no. 10, pp. 3051–3067, May 2019, doi: 10.1175/JCLI-D-18-0810.1.

[12] K. Liou, *An Introduction to Atmospheric Radiation*. New York, NY, USA: Academic, 1980.

[13] A. Slingo, "Sensitivity of the Earth's radiation budget to changes in low clouds," *Nature*, vol. 343, no. 6253, pp. 49–51, Jan. 1990.

[14] C. J. Hahn, W. B. Rossow, and S. G. Warren, "ISCCP cloud properties associated with standard cloud types identified in individual surface observations," *J. Climate*, vol. 14, no. 1, pp. 11–28, Jan. 2001, doi: 10.1175/1520-0442(2001)014<0011:ICPAWS>2.0.CO;2.

[15] S. Manabe and R. F. Strickler, "Thermal equilibrium of the atmosphere with a convective adjustment," *J. Atmos. Sci.*, vol. 21, no. 4, pp. 361–385, Jul. 1964, doi: 10.1175/1520-0469(1964)021<0361:TEOTAW>2.0.CO;2.

[16] S. Manabe and R. T. Wetherald, "Thermal equilibrium of the atmosphere with a given distribution of relative humidity," *J. Atmos. Sci.*, vol. 24, no. 3, pp. 241–259, May 1967.

[17] G. L. Stephens, "Cloud feedbacks in the climate system: A critical review," *J. Climate*, vol. 18, no. 2, pp. 237–273, Jan. 2005, doi: 10.1175/JCLI-3243.1.

[18] D. A. Randall, J. A. Coakley, C. W. Fairall, R. A. Kropfli, and D. H. Lenschow, "Outlook for research on subtropical marine stratiform clouds," *Bull. Amer. Meteorol. Soc.*, vol. 65, no. 12, pp. 1290–1301, Dec. 1984.

[19] A. Bodas-Salcedo et al., "Strong dependence of atmospheric feedbacks on mixed-phase microphysics and aerosol-cloud interactions in HadGEM3," *J. Adv. Model. Earth Syst.*, vol. 11, no. 6, pp. 1735–1758, Jun. 2019.

[20] S. Bony et al., "How well do we understand and evaluate climate change feedback processes?" *J. Climate*, vol. 19, no. 15, pp. 3445–3482, Aug. 2006.

[21] M. D. Zelinka et al., "Causes of higher climate sensitivity in CMIP6 models," *Geophys. Res. Lett.*, vol. 47, no. 1, Jan. 2020, doi: 10.1029/2019GL085782.

[22] T. J. Garrett and C. Zhao, "Ground-based remote sensing of thin clouds in the Arctic," *Atmos. Meas. Techn.*, vol. 6, no. 5, pp. 1227–1243, May 2013, doi: 10.5194/amt-6-1227-2013.

[23] V. Toll, M. Christensen, J. Quaas, and N. Bellouin, "Weak average liquid-cloud-water response to anthropogenic aerosols," *Nature*, vol. 572, no. 7767, pp. 51–55, Jul. 2019.

[24] D. D. Turner, S. A. Clough, J. C. Liljegren, E. E. Clothiaux, K. E. Cady-Pereira, and K. L. Gaustad, "Retrieving liquid Wat0er path and precipitable water vapor from the atmospheric radiation measurement (ARM) microwave radiometers," *IEEE Trans. Geosci. Remote Sens.*, vol. 45, no. 11, pp. 3680–3690, Nov. 2007, doi: 10.1109/TGRS.2007.903703.

[25] M. F. Khairoutdinov and D. A. Randall, "Cloud resolving modeling of the ARM summer 1997 IOP: Model formulation, results, uncertainties, and sensitivities," *J. Atmos. Sci.*, vol. 60, no. 4, pp. 607–625, Feb. 2003.

[26] J. Yuan, Q. Fu, and N. McFarlane, "Tests and improvements of GCM cloud parameterizations using the CCCMA SCM with the SHEBA data set," *Atmos. Res.*, vol. 82, nos. 1–2, pp. 222–238, Nov. 2006, doi: 10.1016/j.atmosres.2005.10.009.

[27] Clothiaux, "An evaluation of a 94-GHz radar for remote sensing of cloud properties," *J. Atmos. Ocean. Technol.*, vol. 12, no. 2, pp. 201–229, Apr. 1995, doi: 10.1175/1520-0426(1995)012<0201:AEOAGR>2.0.CO;2.

[28] P. Kollias, E. E. Clothiaux, M. A. Miller, B. A. Albrecht, G. L. Stephens, and T. P. Ackerman, "Millimeter-wavelength radars: New frontier in atmospheric cloud and precipitation research," *Bull. Amer. Meteorological Soc.*, vol. 88, no. 10, pp. 1608–1624, Oct. 2007, doi: 10.1175/BAMS-88-10-1608.

[29] Z. Wang, Z. Wang, X. Cao, and F. Tao, "Comparison of cloud top heights derived from FY-2 meteorological satellites with heights derived from ground-based millimeter wavelength cloud radar," *Atmos. Res.*, vol. 199, pp. 113–127, Jan. 2018, doi: 10.1016/j.atmosres.2017.09.009.

[30] D. Atlas, "The estimation of cloud parameters by radar," *J. Atmos. Sci.*, vol. 11, pp. 309–317, Aug. 1954, doi: 10.1175/1520-0469(1954)011<0309:TEOCPB>2.0.CO;2.

[31] R. J. P. Baedi, J. J. M. de Wit, H. W. J. Russchenberg, J. S. Erkelens, and J. P. V. Poiares Baptista, "Estimating effective radius and liquid water content from radar and LiDAR based on the CLARE98 data-set," *Phys. Chem. Earth, B, Hydrol., Oceans Atmos.*, vol. 25, nos. 10–12, pp. 1057–1062, Jan. 2000.

[32] N. I. Fox and A. J. Illingworth, "The retrieval of stratocumulus cloud properties by ground-based cloud radar," *J. Appl. Meteorol. Climatol.*, vol. 36, no. 5, pp. 485–492, May 1997, doi: 10.1175/1520-0450(1997)036<0485:TROSCP>2.0.CO;2.

[33] L. P. Liu, R. Zong, Y. B. Qi, and J. Liu, "Microphysical parameters retrieval by cloud radar and comparing with aircraft observation in stratiform cloud," *Eng. Sci.*, vol. 14, no. 9, pp. 64–71, Jun. 2012.

[34] A. S. Frisch, T. Uttal, C. W. Fairall, and J. B. Snider, "On the measurement of stratus cloud properties with a cloud radar and microwave radiometer," in *Proc. IGARSS*, Singapore, Aug. 1998, pp. 2090–2092.

[35] A. S. Frisch, B. E. Martner, I. Djalalova, and M. R. Poellot, "Comparison of radar/radiometer retrievals of stratus cloud liquid-water content profiles with in situ measurements by aircraft," *J. Geophys. Res., Atmos.*, vol. 105, no. D12, pp. 15361–15364, Jun. 2000, doi: 10.1029/2000JD900128.

[36] N. Küchler, S. Kneifel, P. Kollias, and U. Löhnert, "Revisiting liquid water content retrievals in warm stratified clouds: The modified Frisch," *Geophys. Res. Lett.*, vol. 45, no. 17, pp. 9323–9330, Sep. 2018.

[37] P. Sukanya and M. C. R. Kalapureddy, "Cloud microphysical profile differences pertinent to monsoon phases: Inferences from a cloud radar," *Meteorol. Atmos. Phys.*, vol. 131, no. 6, pp. 1723–1738, Mar. 2019.

[38] V. N. Bringi, T. D. Keenan, and V. Chandrasekar, "Correcting C-band radar reflectivity and differential reflectivity data for rain attenuation: A self-consistent method with constraints," *IEEE Trans. Geosci. Remote Sens.*, vol. 39, no. 9, pp. 1906–1915, Sep. 2001, doi: 10.1109/36.951081.

[39] P. V. Hobbs, N. T. Funk, R. R. Weiss, J. D. Locatelli, and K. R. Biswas, "Evaluation of a 35 GHz radar for cloud physics research," *J. Atmos. Ocean. Technol.*, vol. 2, no. 1, pp. 35–48, Mar. 1985.

[40] M. Marzoug and P. Amayenc, "Improved range-profiling algorithm of rainfall rate from a spaceborne radar with path-integrated attenuation constraint," *IEEE Trans. Geosci. Remote Sens.*, vol. 29, no. 4, pp. 584–592, Jul. 1991, doi: 10.1109/36.135820.

[41] M. Marzoug and P. Amayenc, "A class of single- and dual-frequency algorithms for rain-rate profiling from a spaceborne radar. Pad I: Principle and tests from numerical simulations," *J. Atmos. Ocean. Technol.*, vol. 11, no. 6, pp. 1480–1506, Dec. 1994, doi: 10.1175/1520-0426(1994)011<1480:ACOSAD>2.0.CO;2.

[42] P. J. Eccles and E. A. Mueller, "X-band attenuation and liquid water content estimation by a dual-wavelength radar," *J. Appl. Meteorol.*, vol. 10, no. 6, pp. 1252–1259, Dec. 1971, doi: 10.1175/1520-0450(1971)010<1252:XBAALW>2.0.CO;2.

[43] R. J. Hogan, N. Gaussiat, and A. J. Illingworth, "Stratocumulus liquid water content from dual-wavelength radar," *J. Atmos. Ocean. Technol.*, vol. 22, no. 8, pp. 1207–1218, Aug. 2005, doi: 10.1175/JTECH1768.1.

[44] N. Gaussiat, H. Sauvageot, and A. J. Illingworth, "Cloud liquid water and ice content retrieval by multiwavelength radar," *J. Atmos. Ocean. Technol.*, vol. 20, no. 9, pp. 1264–1275, Sep. 2003, doi: 10.1175/1520-0426(2003)020<1264:CLWAIC>2.0.CO;2.

[45] D. Huang, K. Johnson, Y. Liu, and W. Wiscombe, "High resolution retrieval of liquid water vertical distributions using collocated Ka-band and W-band cloud radars," *Geophys. Res. Lett.*, vol. 36, no. 24, Dec. 2009, doi: 10.1029/2009GL041364.

[46] J. Vivekanandan et al., "Cloud microphysics retrieval using S-band dual-polarization radar measurements," *Bull. Amer. Meteorol. Soc.*, vol. 80, no. 3, pp. 381–388, Mar. 1999, doi: 10.1175/1520-0477(1999)080<0381:CMRUSB>2.0.CO;2.

[47] Z. Zhu, K. Lamer, P. Kollias, and E. E. Clothiaux, "The vertical structure of liquid water content in shallow clouds as retrieved from dual-wavelength radar observations," *J. Geophys. Res., Atmos.*, vol. 124, no. 24, pp. 14184–14197, Dec. 2019, doi: 10.1029/2019JD031188.

[48] V. P. Ghate, M. P. Cadeddu, X. Zheng, and E. O'Connor, "Turbulence in the marine boundary layer and air motions below stratocumulus clouds at the ARM eastern North Atlantic site," *J. Appl. Meteorol. Climatol.*, pp. 1495–1510, Sep. 2021, doi: 10.1175/JAMC-D-21-0087.1.

[49] J. Wang et al., "Aerosol and cloud experiments in eastern North Atlantic (ACE-ENA) field campaign report," DOE Office Sci. Atmos. Radiat. Meas. (ARM) Program, Washington, DC, USA, Tech. Rep., DOE/SC-ARM-19-012, 2019.

[50] R. Wood et al., "Clouds, aerosols, and precipitation in the marine boundary layer: An arm mobile facility deployment," *Bull. Amer. Meteorol. Soc.*, vol. 96, no. 3, pp. 419–440, Mar. 2015, doi: 10.1175/BAMS-D-13-00180.1.

[51] Clothiaux, "Objective determination of cloud heights and radar reflectivities using a combination of active remote sensors at the ARM CART sites," *J. Appl. Meteorol.*, vol. 39, no. 5, pp. 645–665, May 2000, doi: 10.1175/1520-0450(2000)039<0645:ODOCHA>2.0.CO;2.

[52] P. Kollias et al., "Development and applications of ARM millimeter-wavelength cloud radars," *Meteorological Monographs*, vol. 57, pp. 1–17, Apr. 2016, doi: 10.1175/AMSMONOGRAPHS-D-15-0037.1.

[53] E. E. Clothiaux et al., "The ARM millimeter wave cloud radars (MMCRs) and the active remote sensing of clouds (ARSCL) value added product (VAP)," DOE, Office Sci. Atmos. Radiat. Meas. (ARM) User Facility, Washington, DC, USA, Tech. Rep. DOE/SC-ARM/VAP-002.1, Mar. 2001.

[54] M. P. Jensen et al., "Contrasting characteristics of open- and closed-cellular stratocumulus cloud in the eastern North Atlantic," *Atmos. Chem. Phys.*, vol. 21, no. 19, pp. 14557–14571, Oct. 2021, doi: 10.5194/acp-21-14557-2021.

[55] J. D. Doviak and D. S. Zrnic, *Doppler Radar and Weather Observations*. San Diego, CA, USA: Academic, 1993.

[56] P. S. Ray, "Broadband complex refractive indices of ice and water," *Appl. Opt.*, vol. 11, no. 8, pp. 44–1836, Aug. 1972, doi: 10.1364/AO.11.001836.

[57] J. Testud, E. Le Bouar, E. Obligis, and M. Ali-Mehenni, "The rain profiling algorithm applied to polarimetric weather radar," *J. Atmos. Ocean. Tech.*, vol. 27, pp. 1906–1951, Mar. 2000, doi: 10.1016/S1464-1909(00)00115-5.

[58] T. F. Coleman and Y. Li, "An interior trust region approach for nonlinear minimization subject to bounds," *SIAM J. Optim.*, vol. 6, no. 2, pp. 418–445, May 1996, doi: 10.1137/0806023.

[59] A. R. Conn, N. I. Gould, and P. L. Toint, *Trust Region Methods*. Philadelphia, PA, USA: Society for Industrial and Applied Mathmatics, 2000.

[60] H. Liu, P. Maghoul, A. Shalaby, A. Bahari, and F. Moradi, "Integrated approach for the MASW dispersion analysis using the spectral element technique and trust region reflective method," *Comput. Geotechnics*, vol. 125, Sep. 2020, Art. no. 103689, doi: 10.1016/j.compgeo.2020.103689.

[61] M. Ahsan and M. A. Choudhry, "System identification of an airship using trust region reflective least squares algorithm," *Int. J. Control, Autom. Syst.*, vol. 15, no. 3, pp. 1384–1393, May 2017, doi: 10.1007/s12555-015-0409-0.

[62] Z. Cui and B. Wu, "A new self-adaptive trust region method for unconstrained optimization," *J. Vibrat. Control*, vol. 18, no. 9, pp. 1303–1309, Aug. 2012, doi: 10.1177/1077546311408473.

[63] M. J. D. Powell, "A new algorithm for unconstrained optimization," in *Nonlinear Programming*, vol. 1970, J. B. Rosen, O. L. Mangasarian, and K. Ritter, Eds. New York, NY, USA: Academic, pp. 31–65.

[64] R. Prasad, U. Mehta, K. Kothari, M. Cirrincione, and A. Mohammadi, "Supercapacitor parameter identification using grey wolf optimization and its comparison to conventional trust region reflection optimization," in *Proc. Int. Aegean Conf. Elect. Mach. Power Electron. (ACEMP) Int. Conf. Optim. Elect. Electron. Equip. (OPTIM)*, 2019, pp. 563–569.

[65] L. Wu et al., "Parameter extraction of photovoltaic models from measured I-V characteristics curves using a hybrid trust-region reflective algorithm," *Appl. Energy*, vol. 232, pp. 36–53, Dec. 2018, doi: 10.1016/j.apenergy.2018.09.161.

[66] A. S. Frisch, C. W. Fairall, and J. B. Snider, "Measurement of stratus cloud and drizzle parameters in ASTEX with a Ka-band Doppler radar and a microwave radiometer," *J. Atmos. Sci.*, vol. 52, no. 16, pp. 2788–2799, Aug. 1995, doi: 10.1175/1520-0469(1995)052<2788:MOSCAD>2.0.CO;2.

[67] W. Zhang et al., "Comparative study of cloud liquid water and rain liquid water obtained from microwave radiometer and micro rain radar observations over central China during the monsoon," *J. Geophys. Res., Atmos.*, vol. 125, no. 20, Oct. 2020, doi: 10.1029/2020JD032456.

[68] P. Wu, X. Dong, B. Xi, J. Tian, and D. M. Ward, "Profiles of MBL cloud and drizzle microphysical properties retrieved from ground-based observations and validated by aircraft in situ measurements over the Azores," *J. Geophys. Res., Atmos.*, vol. 125, no. 9, May 2020, Art. no. e2019JD032205, doi: 10.1029/2019JD032205.

[69] J. Vivekanandan, V. P. Ghate, J. B. Jensen, S. M. Ellis, and M. C. Schwartz, "A technique for estimating liquid droplet diameter and liquid water content in stratocumulus clouds using radar and LiDAR measurements," *J. Atmos. Ocean. Tech.*, vol. 37, no. 11, pp. 1–60, Nov. 2020, doi: 10.1175/JTECH-D-19-0092.1.

[70] X. Huang, Y. Fan, F. Li, H. Xiao, and X. Zhang, "The attenuation correction for a 35 GHz ground-based cloud radar," *J. Infr. Millim. Waves*, vol. 32, no. 4, pp. 325–330, Aug. 2013.

[71] Q. Zheng and M. A. Miller, "Summertime marine boundary layer cloud, thermodynamic, and drizzle morphology over the eastern North Atlantic: A four-year study," *J. Climate*, vol. 35, no. 14, pp. 4805–4825, Jul. 2022.

[72] O. A. Krasnov and H. W. Russchenberg, "Retrieval of water cloud microphysical parameters from simultaneous RADAR and LiDAR measurements," in *Proc. 27th Triennial General Assembly Int. Union Radio Sci.*, vol. 20, no. 3, 2002, pp. 101–115.

[73] L. Liao and K. Sassen, "Investigation of relationships between Ka-band radar reflectivity and ice and liquid water contents," *Atmos. Res.*, vol. 34, pp. 231–248, Sep. 1994, doi: 10.1016/0169-8095(94)90094-9.

[74] O. Pujol, J.-F. Georgis, and H. Sauvageot, "Influence of drizzle on Z–M relationships in warm clouds," *Atmos. Res.*, vol. 86, nos. 3–4, pp. 297–314, Dec. 2007, doi: 10.1016/j.atmosres.2007.06.005.

[75] H. Sauvageot and J. Omar, "Radar reflectivity of cumulus clouds," *J. Atmos. Ocean. Technol.*, vol. 4, no. 2, pp. 264–272, Jun. 1987, doi: 10.1175/1520-0426(1987)004<0264:RROCC>2.0.CO;2.

[76] J. Vivekanandan, B. E. Martner, M. K. Politovich, and G. Zhang, "Retrieval of atmospheric liquid and ice characteristics using dual-wavelength radar observations," *IEEE Trans. Geosci. Remote Sens.*, vol. 37, no. 5, pp. 2325–2334, Sep. 1999, doi: 10.1109/36.789629.

[77] J. Wang and B. Geerts, "Identifying drizzle within marine stratus with W-band radar reflectivity," *Atmos. Res.*, vol. 69, nos. 1–2, pp. 1–27, Oct. 2003, doi: 10.1016/j.atmosres.2003.08.001.

Jinming Ge received the B.E. and Ph.D. degrees in atmospheric science from Lanzhou University, Lanzhou, China, in 2005 and 2010, respectively.

From 2010 to 2012, he was a Lecturer with Lanzhou University, where he became an Associate Professor in 2012 and has been a Professor since 2017. He is currently a Professor with the Key Laboratory for Semi-Arid Climate Change of the Ministry of Education and the College of Atmospheric Sciences, Lanzhou University. His research has focused on atmosphere aerosols, cloud physical properties retrieval, and their radiative effects on climate.

Jiajing Du received the B.E. degree in atmospheric science from Lanzhou University, Lanzhou, China, in 2019, where she is currently pursuing the Ph.D. degree.

Her research interests include radar data processing and cloud physical properties retrieval algorithm.

Zheyu Liang received the B.E. degree in atmospheric science from Lanzhou University, Lanzhou, China, in 2020, where he is currently pursuing the M.S. degree.

His research interests include Ka-band radar signals processing and diurnal variation of precipitation.

Zeen Zhu received the M.S. degree in atmospheric science from Lanzhou University, Lanzhou, China, in 2017, and the Ph.D. degree in atmospheric science from Stony Brook University, Stony Brook, NY, USA, in 2022.

He is currently a Research Associate with the Brookhaven National Laboratory, Upton, NY, USA, and has been a Graduate Research Assistant with the School of Marine and Atmospheric Science, Stony Brook University, since 2017. His research interests include cloud remote sensing and radar applications.

Jing Su received the B.E. and Ph.D. degrees in atmospheric science from Lanzhou University, Lanzhou, China, in 2005 and 2010, respectively.

She is currently an Associate Professor with the Key Laboratory for Semi-Arid Climate Change of the Ministry of Education and the College of Atmospheric Sciences, Lanzhou University. Her research interests include physical properties of cloud and dust aerosols and their radiation effects.

Qinghao Li received the B.S. degree from Lanzhou University, Lanzhou, China, in 2019, where he is currently pursuing the Ph.D. degree.

His research interests include aerosol–cloud interaction and its influence on radiation.

Qingyu Mu received the B.S. degree from the College of Atmospheric Sciences, Lanzhou University, Lanzhou, China, in 2020, where he is currently pursuing the Ph.D. degree, with a focus on contrail cirrus, cloud–aerosol interactions, and atmospheric infrared radiative transfer processes.

Jianping Huang received the Ph.D. degree in weather dynamics from Lanzhou University, Lanzhou, China, in 1988.

He performed post-doctoral work with Peking University, Beijing, China. He is an Academician of the Chinese Academy of Sciences, Beijing, China, and a Professor with the Key Laboratory for Semi-Arid Climate Change of the Ministry of Education and the College of Atmospheric Sciences, Lanzhou University. He is the main author of the first working group of the Working Group I of the Fifth Assessment Report of the Intergovernmental Panel on Climate Change (IPCC) and is one of the academic leaders in the field of atmospheric science in China who has combined systematic observation and theoretical research and made major breakthroughs. He plays an important role in semi-arid climate research in China. He created and developed the first semi-arid climate comprehensive observation station with international standards in western China. His research focuses on the global arid and semi-arid regions and the interaction of dust aerosols with clouds and precipitation.

Qiang Fu received the B.E. and M.S. degrees in atmospheric physics from Peking University, Beijing, China, in 1983 and 1986, respectively, and the Ph.D. degree in atmospheric science from The University of Utah, Salt Lake City, UT, USA, in 1991.

He is currently a Professor of atmospheric sciences with the University of Washington, Seattle, WA, USA. His research interests include light scattering and radiative transfer, atmospheric radiation and clouds, atmospheric aerosols, remote sensing, climate, and climate change.